Soft Matter

Accepted Manuscript

ROYAL SOCIETY OF CHEMISTRY

www.rsc.org/softmatter

Effect of Antimicrobial Peptide on the Dynamics of Phosphocholine Membrane: Role of Cholesterol and Physical State of Bilayer

V.K.Sharma[1,2*], E. Mamontov[3], D. B. Anunciado[1], H. O'Neill[1] and V.S. Urban[1]
[1]*Biology and Soft Matter Division, Neutron Sciences Directorate, Oak Ridge National Laboratory, Oak Ridge, TN 37831, USA*
[2]*Solid State Physics Division, Bhabha Atomic Research Centre, Mumbai 400085, India*
[3]*Chemical and Engineering Materials Division, Neutron Sciences Directorate, Oak Ridge National Laboratory, Oak Ridge, TN 37831, USA*

Abstract

Antimicrobial peptides are universal in all forms of life and are well known for their strong interaction with the cell membrane. This makes them a popular target for investigation of peptide-lipid interactions. Here we report the effect of melittin, an important antimicrobial peptide, on the dynamics of membranes based on 1,2-dimyristoyl-sn-glycero-3-phosphocholine (DMPC) lipid in both the solid gel and fluid phases. To probe the phase transition, elastic neutron intensity temperature scans have been carried out on DMPC-based unilamellar vesicles (ULV) with and without melittin. We have found that addition of a small amount (0.2 mol %) melittin eliminates the steep fall in the elastic intensity at 296 K associated with the solid gel to fluid phase transition, which is observed for pure DMPC vesicles. Quasielastic neutron scattering (QENS) experiments have been carried out on DMPC ULV in the solid gel and fluid phases with and without 0.2 mol % melittin. The data analysis invariably shows the presence of lateral and internal motions of the DMPC molecule. We found that melittin does have a profound effect on the dynamics of lipid molecules, especially on the lateral motion, and affects it in a different way, depending on the phase of the bilayers. In the solid gel phase, it acts as a plasticizer, enhancing the lateral motion of DMPC. However, in the fluid phase it acts as a stiffening agent, restricting the lateral motion of the lipid molecules. These observations are consistent with the mean squared displacements extracted from the elastic intensity temperature scans. Their importance lies in the fact that many membrane processes, including signaling and energy transduction pathways, are controlled to a great extent by the lateral diffusion of lipids in the membrane. To investigate the effect of melittin on vesicles supplemented with cholesterol, QENS experiments have also been carried out on DMPC ULV with cholesterol in the presence and absence of 0.2 mol% melittin. Remarkably, the effects of melittin on the membrane dynamics disappear in the presence of 20 mol % cholesterol. Our measurements indicate that the destabilizing effect of the peptide melittin on membranes can be mitigated by the presence of cholesterol. This study might provide new insights into the mechanism of action of antimicrobial peptides and their selective toxicity towards foreign microorganisms.

Keywords: Antimicrobial peptides, Melittin, Neutron scattering, DMPC, Cholesterol

*Corresponding Author Email: sharmavk@ornl.gov, sharmavk@barc.gov.in

INTRODUCTION

Antimicrobial peptides are a part of the first line of defense against pathogens. They are found among all classes of life, ranging from bacteria to plants, fish, insects, and mammals [1,2]. These peptides serve as therapeutic agents against a wide array of infections and even cancer cells [3]. For the development of therapeutic agents, the selective toxicity is a prerequisite, and the antimicrobial peptides have an edge because they preferentially act on foreign microorganisms while remain harmless to the host cells. For most of the antimicrobial peptides, the cell membrane of the pathogen is the main target. The cell membrane consists of a mixture of lipids, membrane integral proteins, and other small molecules (e.g. cholesterol) which are self-assembled into a heterogeneous structure [4]. Structure and dynamics of cell membranes are susceptible to modification due to interactions with antimicrobial peptides, which has been a subject of interest in biophysics for the last few decades [1-3]. Because the interaction of antimicrobial peptide with cell membrane is particularly complex, simplified systems composed of phospholipids are often used as a model cell membrane. A prototypical antimicrobial peptide, melittin, is the major toxic component in the honey bee venom [5,6]. It is a small linear amphipathic peptide consisting of 26 amino acids, of which residues 1–20 (amino-terminal region) are mostly hydrophobic, while residues 21–26 (carboxy-terminal region) are hydrophilic because of the presence of a stretch of positively charged amino acids. Due to its amphiphatic character, melittin is highly soluble in water (greater than 250 mg/ml) and readily associates with other amphiphilic structures such as lipid bilayers [5,6]. Such a sequence of amino acids, coupled with its amphiphilic nature, is characteristic of many membrane-bound peptides and putative transmembrane helices of membrane proteins [5-7]. This has led to the use of melittin as a popular system for probing lipid-protein interactions in membranes. Since the association of peptides in the membranes is related to physiological effects [6], understanding the details of melittin interaction with membrane components is of much interest. Such understanding becomes still more important since melittin is known to mimic the N terminal of human HIV-1 virulence factor [8], and the alpha-helical conformation of this hemolytic toxin in membranes resembles those of signal peptides [9]. Furthermore, melittin shows similarities in the sequence and structure to a region of the tobacco mosaic virus coat protein (TMV CP) that is crucial for protein–protein and protein–RNA interactions [10]. Due to the aforementioned characteristics and various other interesting properties, such as lysis effect, membrane penetration, antimicrobial

activity, and its voltage-dependent ion conductance, melittin has been one of the most extensively studied antimicrobial peptide. Since melittin approaches target membranes via the aqueous phase, it is the melittin properties in water solutions that are particularly relevant to the effects that melittin exerts on membranes. The conformation of melittin in aqueous solutions is a function of many variables such as concentration, ionic strength, and pH [5,6,11]. At low concentrations, melittin is monomeric and adopts essentially a random coil conformation. However, in the presence of lipid bilayers, the peptide adopts a helical conformation and has the ability to form tetramers [5,6]. Interaction of melittin with a membrane is complex, as melittin may exert several actions, depending on the composition of the bilayer, peptide concentration, bulk solution pH, physical state of bilayer, etc. [5,6]. Melittin is known to induce reorganization of lipid assemblies that may include vesicularization of multibilayers, fusion of small lipid vesicles, pore formation, and fragmentation into micelles. The exerted effects depend on the experimental conditions, such as peptide/lipid ratio, temperature, etc. [5,6,12]. Remarkably, micellization of melittin specifically takes place in membranes composed of pure saturated phosphatidylcholines (PC) and shows an interesting dependence on the solid gel to fluid phase transition temperature (T_m) [13,14]. In the fluid phase, bilayers are stable as extended liposomes at melittin concentrations of up to 5 mol%. However, as the temperature is decreased into the gel phase region, melittin induces the transmembrane pores and subsequently disrupts liposome into small disk shaped micelles. This bilayers conversion into micelles has been shown to be reversible as the gel phase micellar discs re-amalgamate to form the extended bilayer when the temperature is raised above the lipid phase transition temperature (T_m) [12-14]. It seems unlikely that a single molecular model could account for all the observed phenomena. Melittin could thus illustrate many scenarios in biological systems, and it provides, from a physico-chemical point of view, an attractive model to reveal the mechanism of lipid-protein interactions at the molecular level. The effect of inclusion of melittin in lipid bilayer on the structural properties has been well studied and reported [5,6, 12,14-19]. However, the effect on the dynamical behavior of lipid bilayer has not been widely studied. Studies of dynamical behavior of lipids are of significance from the standpoint of both basic science and industrial applications. Dynamics of lipid molecules in the bilayer can be studied experimentally using various techniques, such as nuclear magnetic resonance (NMR) [20-22], fluorescence spectroscopy [23], and inelastic neutron scattering [24-32]. Most techniques are only capable of monitoring the dynamics on a restricted

time and length scale [33]. Inelastic neutron scattering possesses advantage over other techniques due to an additional experimental parameter, wave vector transfer, *Q*, which yields spatial information on the geometry of the motion. The neutron spin echo technique, which is capable of monitoring the slowest molecular time scale among the dynamic neutron scattering techniques (as slow as hundreds of nanoseconds), has been recently employed to study the effect of addition of melittin on the bending elasticity of dioleoyl-phosphocholine (DOPC) bilayer, in the fluid phase [32]. However, there is not much information available on the effect of melittin on the local dynamics of individual lipid molecules in both the solid gel and fluid phases, which can be studied experimentally using Quasi Elastic Neutron Scattering (QENS). QENS is an ideal technique for observing molecular motions on a pico- to nanosecond timescale and on a length scale from Angstroms to tens of nanometers [24-31, 34-39]. Recently, we have employed QENS to study the relationship of the solid gel to fluid phase transition with the dynamics of 1,2-dimyristoyl-sn-glycero-3-phosphocholine (DMPC) unilamellar vesicles [39]. Our results show that both lateral as well as internal motions of DMPC molecules change dramatically at the main phase transition. The lateral motion of DMPC molecules becomes an order of magnitude faster in the fluid phase, while the internal motion shows changes not only in the time scale, but also in the geometry [39].

Cholesterol is a vital component of eukaryotic membranes that plays a critical role in membrane organization, dynamics, function, and sorting [40-42]. The rigid ring system and the orientation perpendicular to the membrane can make cholesterol an attractive target for many bacterial toxins and fungal antibiotics [43]. The importance of the melittin-cholesterol interaction can be appreciated from the fact that the erythrocyte membrane, which is the natural target for melittin, contains high amounts (up to 45 mol %) of cholesterol [5,6,10] Comparing the results obtained from addition of melittin in cholesterol-free bilayer and cholesterol-supplemented bilayers provides us with insights into the role played by cholesterol in lipid-melittin interactions.

Here, we present neutron elastic intensity temperature scans and QENS experiments on unilamellar vesicles (ULV) of neat DMPC and DMPC with cholesterol in the presence and absence of melittin. QENS experiments were carried out in both the solid gel and fluid phases to investigate the role of the physical state of the bilayer in the interaction with melittin. We discuss new findings on the dynamics of lipid molecules with respect to the presence of melittin and its strong dependence on the physical state and composition of the bilayer.

MATERIALS and METHODS

Materials

The phospholipid dimyristoylphosphatidylcholine (DMPC) was procured from Avanti Polar Lipids (Alabaster, AL) in powder form. Melittin and cholesterol were obtained from Sigma Aldrich (St. Louis, MO). D_2O (99.9%) was purchased from Cambridge Isotope Laboratories (Andover, MA). All materials were used as provided.

Unilamellar Vesicles Preparation

DMPC Lipid powders with and without 20 mol % cholesterol (with respect to the total number of lipid and cholesterol molecules) were dissolved in the appropriate amount of chloroform. This concentration of cholesterol was chosen because the natural target for melittin is the erythrocyte membrane, which contains high amounts of cholesterol, up to 45 mol % [5,40]. Chloroform was evaporated using a gentle stream of nitrogen gas to obtain lipid films. The lipid films were dried to remove residual organic solvent by placing the samples under vacuum (10^{-3} atm) for 15 hrs at 310 K. The dried lipid films, with and without cholesterol, were hydrated by dissolving them in D_2O to form vesicles. These lipid suspensions were subjected to more than four freeze-thaw cycles by alternately placing the suspension in a warm water bath (320 K) and in a freezer (253 K). The vesicles were extruded by passing the suspension more than 25 times through a mini-extruder from Avanti Polar Lipids (Alabaster, AL) fit with a porous polycarbonate membrane (pore diameter ~100 nm). During the extrusion process, the extruder was placed on a hot plate set at 320 K, well above the DMPC gel−fluid phase transition temperature. The concentration of the melittin stock solution was determined spectrophotometrically using the extinction coefficient, ε_{280nm}=5570 M^{-1} cm^{-1} [44] with a Shimadzu UV-2700 UV-visible spectrophotometer. To incorporate melittin into membranes, an appropriate amount of melittin stock solution was added to the vesicles solution at 310 K and mixed well. The final concentration of vesicles solution was kept at 74 mM of DMPC with and without melittin 0.2 mol % with respect to lipid molecules. There were 4 ULV samples prepared: (i) 74 mM DMPC (ii) 74 mM DMPC with 0.2 mol % melittin (iii) 74 mM DMPC with 20 mol% cholesterol and (iv) 74 mM DMPC with 20 mol% cholesterol and 0.2 mol % melittin.

Circular Dichroism

Circular dichroism (CD) spectroscopy was performed using a JASCO J-810 spectropolarimeter to verify the association of melittin with the vesicles by measuring the secondary structure of melittin. CD measurements were carried out on melittin in pure D_2O, in DMPC vesicles, and in DMPC vesicles containing cholesterol at 310 K. The spectra were recorded with a scan speed of 100 nm/min, 0.25s response time, and a bandwidth of 1 nm from 190–250 nm. Each spectrum presented is an average of 5 scans. The secondary structure content of the samples was quantified using the CD Pro program with the CONTIN method and STR43 basis set [45].

Neutron Scattering Experiments

Elastic incoherent neutron scattering (EINS) is one of the best suitable techniques [46-47] to investigate the onset of motion or phase transitions. In EINS or an elastic intensity scan, the scattering intensity centered at zero energy transfer is measured as a function of temperature. Two kinds of measurements, namely EINS and QENS, were carried out on all four aforementioned vesicles solutions (with and without cholesterol/melittin) using the high resolution backscattering spectrometer, BASIS [48] at the Spallation Neutron Source (SNS), Oak Ridge National Laboratory (ORNL). For the chosen experimental setup, the BASIS had an energy resolution of 3.4 μeV (full width at half-maximum, for the *Q*-averaged resolution value), and an energy transfer window suitable for analysis was ±100 μeV. The samples were placed in annular aluminum cans with an internal spacing of 0.5 mm chosen to achieve no more than 10% scattering and thus reduce multiple scattering. The elastic intensity scans were carried out as a function of temperature from 305 to 260 K (i.e., on cooling), with a step of 1 K. QENS data were collected in the *Q* range of 0.3 $Å^{-1}$ to 1.5 $Å^{-1}$. QENS measurements were carried out at two different temperatures, 280 and 310 K, where pure DMPC lipids are known to be in the solid gel and fluid phase, respectively. QENS measurements were also carried out on pure D_2O at 280 K and 310 K as a reference sample. For the instrument resolution, QENS measurements were carried out on all four vesicles solutions at 10 K. MANTID software [49] was used to carry out standard data reduction, which included background subtraction and detector efficiency corrections. No multiple scattering and self-shielding corrections have been used in the data reduction.

QENS DATA ANALYSIS

Incoherent scattering cross section of hydrogen atom exceeds by two orders of magnitude than the coherent or incoherent scattering cross section of any other atoms. Here, we are interested in the dynamics of hydrogenated lipid-based vesicles in solution, and thus use D_2O to minimize the scattering contribution from the solvent. Spectra from the pure D_2O were also recorded and subtracted from those measured for the vesicle solutions rather than being modeled with a separate scattering function. The signals were first normalized to the incident beam monitor counts, and then the final scattered intensity from the vesicles, $I_{\text{vesicles}}(Q,\omega)$, was obtained using the following relation,

$$I_{vesicles}(Q,\omega) = I_{solution}(Q,\omega) - \phi I_{D_2O}(Q,\omega) \quad (1)$$

where ϕ is the volume fraction of D_2O. The so reduced data are proportional to the dynamic structure factor of the system of vesicles, but not expressed in the absolute units. On the other hand, the model scattering functions that we discuss in detail below, $S_{vesicles}(Q,\omega)$, are expressed in the units of inverse energy. Thus, following the standard practice of QENS data fitting, a scaling constant was used as one of the fit parameters.

To proceed with the data analysis, it is customary to separate the contribution from different kinds of motions according to their time scales. It is assumed that these contributions are independent of each other. As mentioned earlier, QENS is a suitable technique for studying motions on the nanosecond to picoseconds time scale. In this time scale range, the lipid molecules have freedom to undergo lateral motion within the monolayer (~ns), the segmental or internal motion (~ps), and the fast torsional motion (~sub ps) [24,30]. BASIS (ΔE=3.4 μeV and energy transfer range ± 100 μeV) is one of the best suited spectrometer to study lateral (~ns) as well as internal motions (~ps) of the vesicle, which is of our current interest [24,30,39]. However, fast torsional motion (~sub ps) will not be observable due to limited energy transfer range and will contribute to the background. Therefore, the model scattering law for the vesicles can be expressed as

$$S_{vesicles}(Q,\omega) = \left[S_{lat}(Q,\omega) \otimes S_{\text{int}}(Q,\omega)\right] \quad (2)$$

where $S_{lat}(Q,\omega)$ and $S_{int}(Q,\omega)$ correspond to the scattering functions due to the lateral and internal motions of the lipid molecules, respectively. The lateral motion is well characterised by continuous flow diffusion [26,27] and therefore, the scattering law for the lateral motion can be written as

$$S_{lat}\left(\mathrm{Q},\omega\right) = L_{lat}(\Gamma_{lat},\omega) = \frac{1}{\pi}\frac{\Gamma_{lat}}{\Gamma_{lat}^2+\omega^2} \tag{3}$$

Here Γ_{lat} is the half width at half maximum (HWHM) of the Lorentzian corresponding to the lateral motion of the lipid molecules.

The internal motions are localized, and, therefore, the scattering law for the internal motion, $S_{int}(Q,\omega)$ can be expressed as

$$S_{\mathrm{int}}\left(Q,\omega\right) = A\left(Q\right)\delta\left(\omega\right) + \left(1-A\left(Q\right)\right)L_{\mathrm{int}}(\Gamma_{\mathrm{int}},\omega) \tag{4}$$

where the first term represents the elastic component and second term represents the quasielastic component approximated by a single Lorentzian function, $L_{\mathrm{int}}(\Gamma_{\mathrm{int}},\omega)$ with a half width at half maximum (HWHM), Γ_{int},. $A(Q)$ is known as Elastic Incoherent Structure Factor (EISF) which is the fraction of the elastic scattering with respect to the total scattering. From Eqs. (3) and (4), the scattering law for vesicles can be written as

$$\begin{aligned} S_{vesicles}\left(Q,\omega\right) &= L_{lat}(\Gamma_{lat},\omega)\otimes\left[A\left(Q\right)\delta\left(\omega\right)+\left(1-A\left(Q\right)\right)L_{\mathrm{int}}(\Gamma_{\mathrm{int}},\omega)\right] \\ &= \left[A\left(Q\right)L_{lat}\left(\Gamma_{lat},\omega\right)+\left(1-A\left(Q\right)\right)L_{tot}(\Gamma_{tot},\omega)\right] \end{aligned} \tag{5}$$

Here, the Lorentzian, $L_{tot}(\Gamma_{tot},\omega)$ represents the combination of the lateral and internal motions of the lipid molecules, where $\Gamma_{tot} = \Gamma_{lat} + \Gamma_{\mathrm{int}}$. The above scattering law (Eq. (5)) was convoluted with the instrumental resolution function, and the parameters *A(Q)*, Γ_{lat} and Γ_{tot} were determined by a least squares fit of the measured spectra. The data were fitted using the program DAVE [50] developed at the NIST Center for Neutron Research.

Model for Internal Motions

Lipid molecules have a complex structure with a number of hydrogen atoms, which makes it difficult to perform quantitative analysis of the internal motion. However, such

analysis becomes possible using some approximations [39], which enable us to extract meaningful physical parameters. Recently, we have successfully described the internal motion of DMPC molecules in unilamellar vesicles in both the solid gel and fluid phases [39]. In the solid gel phase, a fractional uniaxial rotational model, in which a fraction of hydrogen atoms of the acyl chain underdo rotation on a circle with a radius *r*, has been used to describe the internal motion of DMPC molecules. The scattering law for fractional uniaxial rotational motion can be written as [31,39,51]

$$S_{\text{int}}(Q,\omega) = (1-p)\delta(\omega) + p\left[B_0(Qr)\delta(\omega) + \frac{1}{\pi}\sum_{n=1}^{N-1} B_n(Qr)\frac{1/\tau_n}{(1/\tau_n)^2+\omega^2}\right] \quad (6)$$

With
$$B_n(Qr) = \frac{1}{N}\sum_{p=1}^{N} j_0(2Qr\sin\frac{\pi p}{N})\cos(\frac{2\pi np}{N}) \quad (7)$$

$$\tau_n^{-1} = D_r\frac{\sin^2(n\pi/N)}{\sin^2(\pi/N)} \quad (8)$$

where *p* is the fraction of mobile hydrogen atoms, *N* is number of sites equally distributed on a circle of radius *r*, j_0 is spherical Bessel function of the zeroth order, and D_r is rotational diffusion constant. Resultant EISF for the fractional uniaxial rotational model becomes

$$A_{L_\beta}(Q) = (1-p) + p\frac{1}{N}\sum_{q=1}^{N} j_0(2Qr\sin\frac{\pi q}{N}) \quad (9)$$

A summation for N=12, a large enough number (>6), is found to be adequate for adopting the uniaxial rotational diffusion model for the *Q*-range used here.

However, in the fluid phase, a localized translational diffusion model, in which the hydrogen atoms corresponding to the different CH_2 units of the acyl chain diffuse with varying diffusivities within spheres of varying radii, is found to be more appropriate to describe the observed internal motion [39]. In this model, the radius of the sphere and the diffusivity increase linearly along the acyl chain, in such a manner that the hydrogens near to the polar head group move within the spheres having smaller volume with lower diffusion constant than the hydrogens away from the head group. The scattering law for this model can be written as [39,52]

$$S_{\text{int}}(Q,\omega) = \frac{1}{M}\sum_{i=1}^{M}\left[\left[\frac{3j_1(QR_i)}{QR_i}\right]^2\delta(\omega) + \frac{1}{\pi}\sum_{\{l,n\}\neq\{0,0\}}(2l+1)A_n^l(QR_i)\frac{(x_n^l)^2 D_i/R_i^2}{\left[(x_n^l)^2 D_i/R_i^2\right]^2+\omega^2}\right] \quad (10)$$

where $A_n^l(QR_i)$ (n, $l \neq 0,0$) is the quasielastic structure factor and the values for $A_n^l(QR_i)$ for different n and l can be calculated by using the values of x_n^l listed in Ref. 52. R_i and D_i are the radius of the sphere and associated diffusivity at the i^{th} site of the acyl chain from the polar head towards tail and can be written as

$$R_i = \frac{i-1}{M-1}\left[R_{\max} - R_{\min}\right] + R_{\min} \quad (11)$$

and

$$D_i = \frac{i-1}{M-1}\left[D_{\max} - D_{\min}\right] + D_{\min} \quad (12)$$

where M is the total number of CH_2 units in the acyl chain that are contributing to the observed dynamics. For DMPC M is equal to 14. In this model, the hydrogens of the first CH_2 unit (nearest to the polar head group) will undergo localised diffusion within the smallest sphere of radius R_{min} and with the minimum diffusion coefficient D_{min}. As one moves progressively from the polar head group along the acyl chain, both the radius of the sphere and the diffusivity increase and the hydrogens at the end of the hydrophobic tail (CH_3) will generate the largest size sphere of radius R_{max} and with maximum diffusion coefficient D_{max}. The resultant EISF for this model can be written as

$$A_{L_\alpha}(Q) = \frac{1}{14}\sum_{i=1}^{14}\left[\frac{3j_1(QR_i)}{QR_i}\right]^2 \quad (13)$$

RESULTS AND DISCUSSION

Circular Dichroism

The far-UV CD spectra of the samples were measured to determine the secondary structural changes of melittin in the presence of DMPC and DMPC with cholesterol. In D_2O, melittin shows a spectrum typical for a random coil or unfolded protein [53], this is characterized by a minimum near 200 nm (Fig. 1). However, in the presence of DMPC, melittin shows two minima around 208 nm and 222 nm consistent with an α-helical conformation of melittin [53], indicating that it is associated with the membrane. It is evident from Fig. 1 that the presence of cholesterol in the vesicles affect the interaction of melittin with DMPC as CD spectra get shifted towards

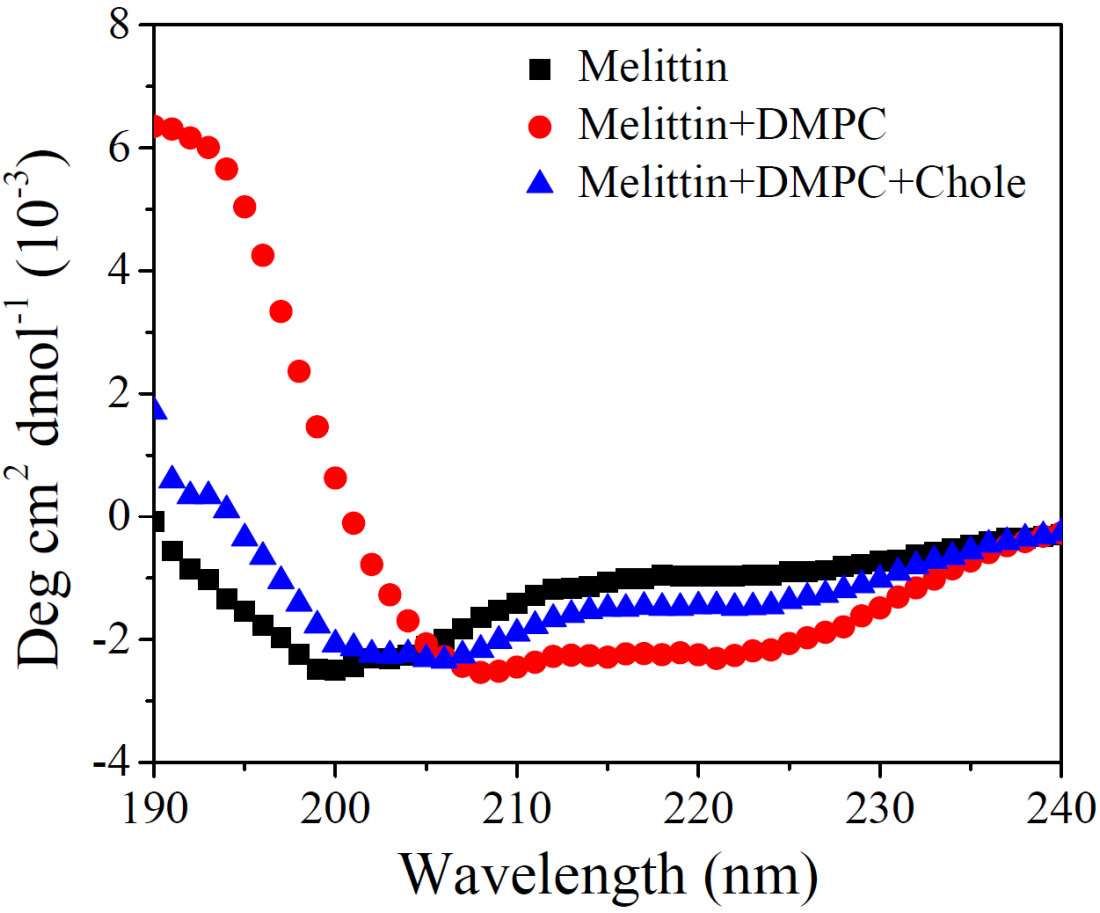

Fig. 1. A comparison of the far-UV circular dichroism spectra of melittin in pure D_2O (black), in DMPC ULV (red) and in DMPC ULV with 20 mol % cholesterol (blue) at 310K.

lower wavelength and the depth of the minima also decrease. This indicates that melittin undergoes less folding with less helical conformation in DMPC/cholesterol vesicles compared to DMPC vesicles. The alpha-helical content in the structure was estimated using CONTIN/ SDP48 basis set analysis [45]. In D_2O, melittin has ~ 19 % helical content which was found to increase to ~68% in the presence of DMPC vesicles. In the case of DMPC vesicles with cholesterol, the helical content is only ~32%, indicating less interaction of melittin with membrane. Table 1 shows the detailed secondary structural analysis of melittin in D_2O, in DMPC vesicles, and in DMPC vesicles with cholesterol.

Table 1. The secondary structure analysis of melittin in D_2O, in DMPC vesicles and in DMPC vesicles with Cholesterol using CD Pro analysis (CONTIN/SDP48).

Sample	α-Helical	β-Sheet	β-Turn	Random coil	NRMSD
Melittin	0.19	0.01	0.08	0.72	0.039
Melittin-DMPC	0.68	0.04	0.08	0.20	0.024
Melittin-DMPC-Chol	0.32	0.02	0.16	0.50	0.060

EINS and QENS

Vesicles without Cholesterol:

Elastic intensity temperature scans probe the mobility in samples by determining the amount of elastic scattering as a function of temperature within the experiment resolution window. The elastic intensity is sensitive to the dynamical processes, since the excitation of the dynamical modes shifts the scattering intensity away from zero energy transfer. An abrupt loss of intensity in elastic scan experiment is an indication of a phase transition associated with a change in the dynamics at the respective temperature. Fig. 2a shows the elastic intensity (integrated over the energy transfer range of ±3.4 μeV) for DMPC ULV solutions in the presence and absence of melittin summed over all accessible scattering angles in the temperature range from 260 to 305 K. The transition near 270 K corresponds to freezing of heavy water. Here, we focus on the temperature range near the main phase transition of lipids, i.e., ~ 296 K, which is magnified and shown in the inset. It is evident that in the case of pure DMPC vesicles, the elastic intensity decreases linearly with increasing temperature up to 296 K, and a subsequent step-like fall in the

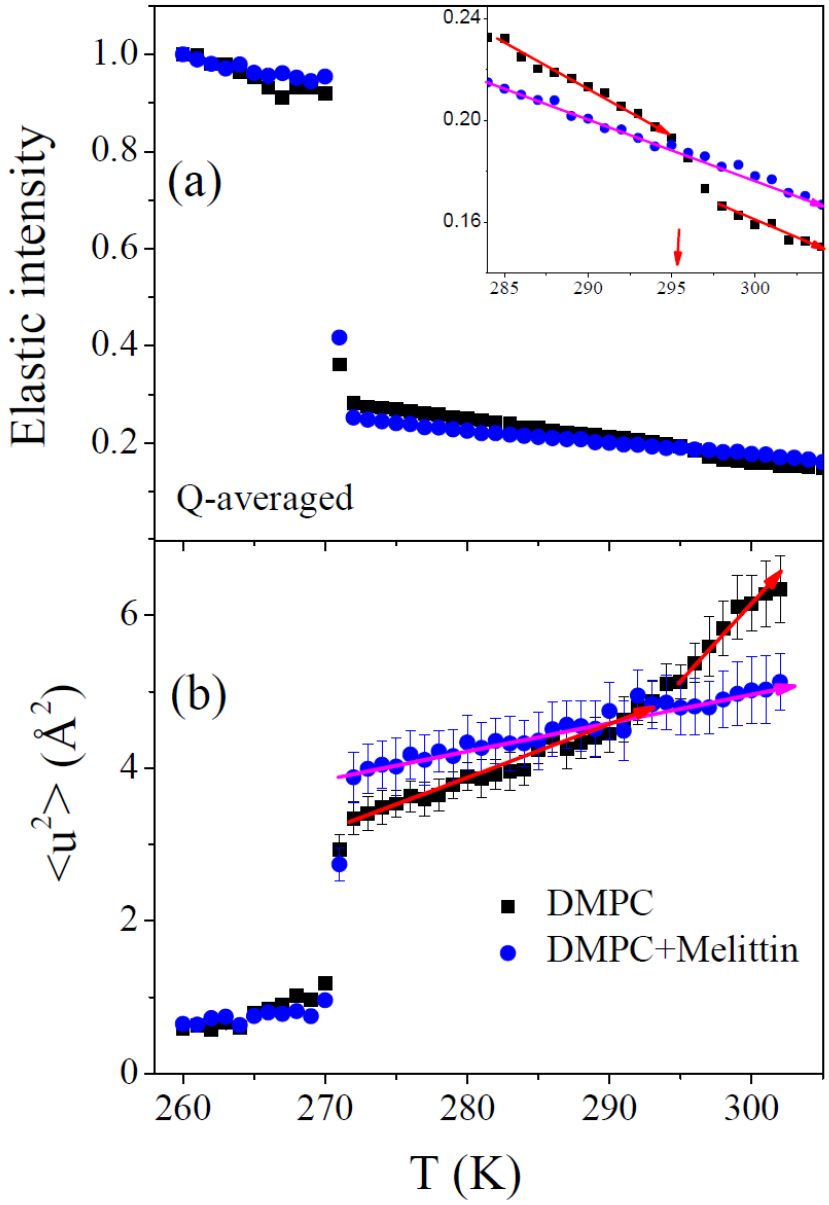

Fig. 2 Temperature dependence of the (a) *Q*-averaged elastic intensity and (b) average mean square displacement $\langle u^2 \rangle$ for 74 mM DMPC ULV in the absence and presence of 0.2 mol% melittin. A region around the main phase transition temperature of DMPC (~296 K) for the *Q*-averaged intensity is magnified and shown in the inset. It is evident that in the case of DMPC ULV, there is a sudden change in the behavior of elastic intensity and in $\langle u^2 \rangle$ around 296 K, which corresponds to the solid gel to fluid phase transition of DMPC. However, inclusion of 0.2 mol % melittin inhibits this main phase transition. Solid red and magenta lines are drawn as guides to the eye.

intensity indicates the existence of the solid gel to fluid phase transition. However, inclusion of 0.2 mol % melittin is found to eliminate the steep fall in the elastic intensity at 296 K (inset of Fig. 2a), which indicates that the presence of a small amount of melittin does have a profound effect on the main solid gel to fluid phase transition. These results are found to be consistent with an earlier differential scanning calorimetry (DSC) study [54] which indicates that addition of melittin leads to a significant broadening (more than 20 K) of the main phase transition peak (~296 K).

Average mean-squared displacement (MSD), $\langle u^2 \rangle$ can be extracted from EINS by assuming the Gaussian approximation to the *Q*-dependence of the elastic neutron scattering intensity (where *Q* is the magnitude of the scattering vector) using the following Eq.

$$\ln\left[\frac{I_{el}(Q,T)}{I_{el}(Q,T_{\min})}\right] = -\frac{\langle u^2 \rangle Q^2}{6} \qquad (14)$$

To obtain $\langle u^2 \rangle$, the *Q*-dependent elastic intensities are normalized to the lowest measured temperature 10 K data and fitted with Eq. (14) in the *Q* range of 0.3 to 1.0 Å^{-1}. The so obtained mean squared displacements ($<u^2>$) for pure DMPC ULV and DMPC with melittin ULV are shown in Fig. 2b. It is evident that in the case of pure DMPC ULV, there is a change in the slope of the MSD at and around the main transition temperature (296 K). However, no such change in slope is observed for DMPC ULV containing melittin. This observation is consistent with the elastic intensity scan, which indicates that the inclusion of melittin inhibits the main phase transition. Moreover, an interesting behaviour of $<u^2>$ is observed; it is found that below the phase transition temperature (< 296 K), i.e., in the solid gel phase, the average mean square displacement for neat DMPC is lower than that observed for DMPC having melittin. However, in the fluid phase (>296 K), i.e. above the main phase transition, this trend gets reversed, i.e., $<u^2>$ for pure DMPC ULV is higher than for DMPC ULV containing melittin. This indicates that inclusion of melittin has an interesting opposite effect on $\langle u^2 \rangle$ depending on the phase state of bilayer.

QENS spectra for the DMPC vesicle with and without 0.2 mol % melittin in the solid gel (280K) and fluid phase (310K) are obtained using Eq. (1). The spectra are normalized to the peak intensities and shown in Fig 3a and b for the solid gel and fluid phases, respectively, at a typical *Q* value of 0.9 Å^{-1}. The instrumental resolution, as measured using the pure DMPC vesicles solution at 10 K, is also shown for comparison. It is evident from Fig. 3 that DMPC ULVs with

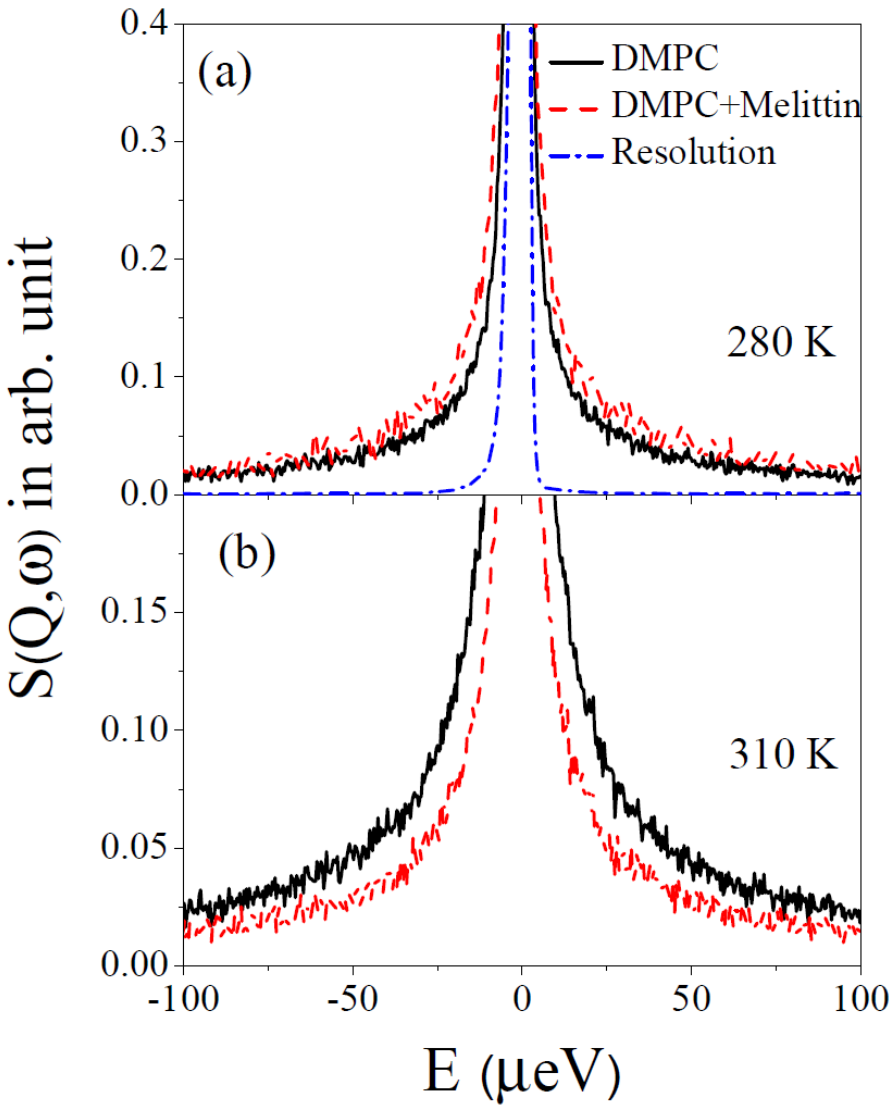

Fig. 3 Typical observed QENS spectra for 74 mM DMPC vesicles in the presence and absence of 0.2 mol % melittin at Q=0.9 Å^{-1} in (a) solid gel phase at 280 K and (b) fluid phase at 310 K. The instrument resolution is shown by the dash-dotted line in upper panel. The contribution of the solvent (D_2O) has been subtracted using Eq. (1) and the resultant spectra are normalized to the peak amplitudes.

and without 0.2 mol % melittin shows significant quasielastic (QE) broadening over the instrumental resolution in both the solid gel and fluid phases. It is evident that in the solid gel phase, DMPC vesicles with melittin show broader quasielastic signal compared to pure DMPC vesicles, indicating relatively faster dynamics of lipids in the presence of melittin. However, in the fluid phase, the addition of melittin acts in the completely opposite direction, leading to

decrease in the width of the quasielastic signal compared to pure vesicles. These QENS results are in full agreement with the MSD data as presented in Fig. 2b. Our observations suggest that the interaction mechanism of melittin with the lipid bilayer greatly depends on the physical state of the bilayer, indicating that addition of melittin (0.2 mol%) affects dynamics in a profoundly different way, depending on the phase of lipid bilayer. The observed QENS spectra for DMPC vesicles with and without melittin in both solid gel and fluid phases are described well by the model function (Eq. (5)) at all Q values. A typical fitted spectrum for DMPC vesicles with melittin in the fluid phase is shown in Fig. 4. To gain more insight into the nature of the two dynamical processes, the parameters obtained from the fit are analysed as a function of Q. The lateral motion of the entire lipid molecules will be slower than the internal motion [24,30,39]. Therefore, the narrower Lorentzian (hereafter referred as 1st Lorentzian) will correspond to the lateral motion, whereas the broader Lorentzian (hereafter referred as a 2nd Lorentzian) represents the convolution of two Lorentzians, corresponding to the superposition of the lateral and internal motions of the lipid molecules.

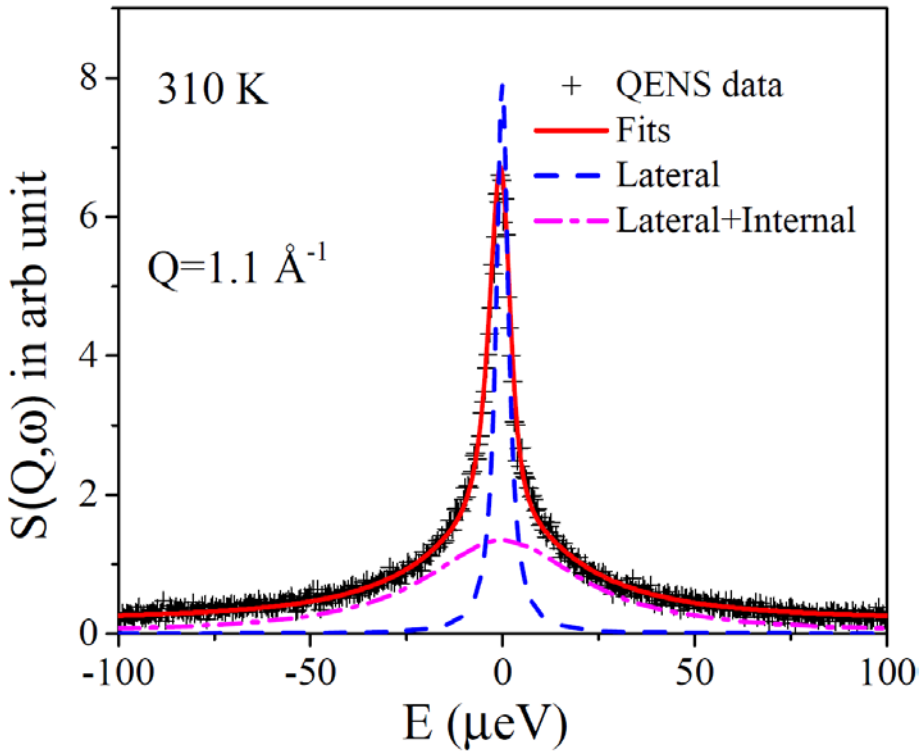

Fig. 4 Typical fitted $S_{vesicles}(Q, \omega)$ for 74 mM DMPC vesicles with 0.2 mol % melittin at 310 K assuming the model scattering function given by Eq. (5). The contribution from the solvent (D_2O) has been subtracted using Eq. (1).

The variation of the HWHM of the 1st Lorentzian, Γ_{lat}, with Q^2 for DMPC ULV in the presence of 0.2 mol % melittin is shown in Fig. 5 at 280 and 310 K. For one to one comparison, Γ_{lat}, observed for DMPC ULV [39] is also shown in Fig. 5 at 280 and 310 K. It is evident that for DMPC vesicles with and without 0.2 mol % melittin, Γ_{lat} varies linearly with Q^2 at both temperatures, consistent with continuous Brownian diffusion. Γ_{lat} is described well by a simple Brownian motion using Ficks law, HWHM=$D_{lat}Q^2$, as shown by the solid lines in Fig. 5. Here D_{lat} is the diffusion coefficient for the lateral motion of the lipid molecules obtained from the slope of the straight line fit. In the solid gel phase, i.e., at 280 K, the lateral diffusion coefficient of DMPC molecules in ULV is found to be $(0.7 \pm 0.1) \times 10^{-7}$ cm^2/sec, which increases to $(1.1 \pm 0.1) \times 10^{-7}$ cm^2/sec with inclusion of melittin. At 310 K (in the fluid phase), the lateral diffusion coefficient of DMPC molecules in the ULV is $(7.7 \pm 0.3) \times 10^{-7}$ cm^2/sec, which reduces significantly to $(2.4\pm 0.1) \times 10^{-7}$ cm^2/sec with addition of melittin. It is evident that inclusion of melittin does have a significant effect on the lateral motion of lipid molecules and acts oppositely depending on the phase of the bilayer. If lipid molecules are in solid gel phase, inclusion of melittin leads to enhancement of the lateral motion; thus, melittin acts as a plasticizer. On the contrary, in the fluid phase, addition of melittin acts in the opposite way, much reducing the lateral diffusion coefficient, i.e., melittin acts as a stiffening agent. This is consistent with the results obtained from the elastic intensity scans described above, which show that the average mean square displacement for DMPC vesicles with melittin is higher in the solid gel phase and lower in the fluid phase compared to pure DMPC vesicles.

Based on our results, it may be argued that the interaction mechanism of melittin with the lipids is quite different in the solid gel and fluid phases. This observation is supported by a recent fluorescence and cryo-TEM study [14], which indicates that in the fluid phase, melittin is distributed homogenously in the lipid bilayer. However, as the temperature is lowered into the solid gel phase, melittin becomes distributed rather heterogeneously, and starts to agglomerate. Such heterogeneous distribution may lead to formation of transmembrane pores. Earlier study [54] also suggested that affinity for melittin with phosphatidylcholine bilayer had a strong

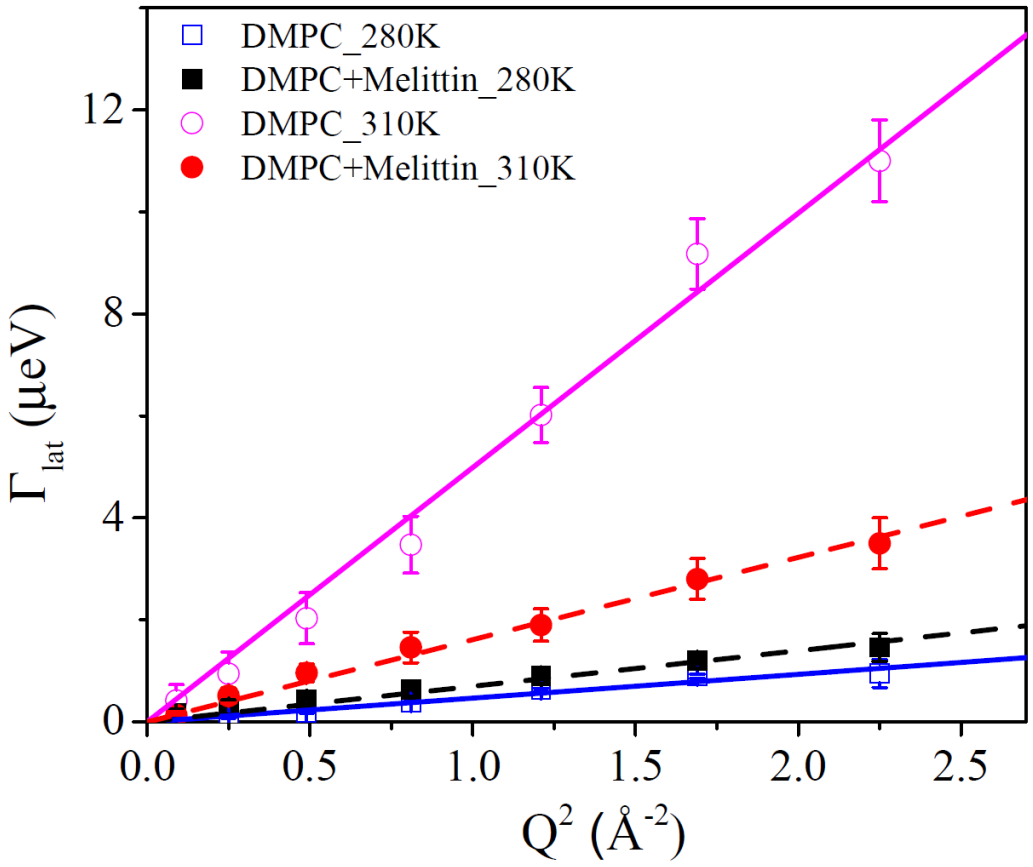

Fig. 5 Variation of the half width at half maximum corresponding to the lateral motion, $\Gamma_{lat,}$ with Q^2 for DMPC vesicles in the presence of 0.2 mol% melittin in both the solid gel (280 K) and fluid (310 K) phase. For comparison, Γ_{lat} as observed for pure DMPC vesicles [39] is also shown here. The solid lines are the fits with Fick's law of diffusion.

dependence on the physical state of the bilayer, in the gel phase, it was found to be much weaker than in fluid phase. The observed QENS results therefore can be explained as follows. In the fluid phase, at such a low peptide to lipid ratio, melittin is distributed homogenously and preferentially lie parallel to the membrane surface [14, 16]. In this case, a large number of lipid molecules experience direct interaction with melittin, which may cause hindrance in the lateral motion of lipid molecules involving the motion of the whole lipid molecules along the leaflet. However, in the gel phase melittin starts to agglomerate, which may cause the formation of transmembrane pores in the vesicles [14]. Melittin is known to form toroidal pores in the vesicles, in which bilayer bends sharply inward to form a pore lined by both peptides and lipid

head groups [55,56]. In this case, very few lipid molecules interact directly with the melittin. Moreover, the formation of pores breaks the long range ordering of the lipid molecules, as was found in the gel phase of neat DMPC vesicles. Such morphological change disturbing the packing of lipid molecules could be the responsible for the enhanced lateral motion in the gel phase.

Our QENS data indicates that, along with the lateral motion, there exists a faster internal motion of the lipid molecule. Internal motion of DMPC vesicles in solid gel and fluid phases has been successfully described by us using uniaxial rotational and localized translational diffusion models respectively [39]. The *Q*-dependence of EISF ($A(Q)$) and the HWHM (Γ_{int}) associated with the internal motions of DMPC vesicles in the presence of 0.2 mol% melittin are shown in figures 6 and 7 respectively. The fractional uniaxial rotational diffusion model (Eq. (9)) describes well the variation of EISF with *Q* as shown by the solid black line. The radius of rotation (r) and the fraction of mobile hydrogens (p) are found to be 2.13 Å and 58% respectively, indicating that 58 % of the hydrogen atoms in the acyl chain are participating in the uniaxial rotation motion on a circle having radius 2.13 Å. It may be noted that in the case of pure DMPC vesicles [39], the radius of rotation (r) and the fraction of mobile hydrogens (p) are found to be 1.78 Å and 58 % respectively. Thus, addition of melittin leads to a slight increase in the radius of rotation, indicating enhanced flexibility of acyl chains in the presence of melittin relative to the neat solid gel phase. Our observations are consistent with the fluorescence and Raman study by Dasseux et al. [54] indicating that in the solid gel phase addition of melittin decreases the fraction of *trans* conformation and intermolecular order of the lipid chains. The uniaxial rotational diffusion model (Eqs. (6) to (8)) is used to describe the variation of Γ_{int} with D_r as a parameter. Fig. 7 shows that this model provides a good description of the observed Γ_{int} at 280 K, and the D_r is found to be 16±2 μeV. By comparison, D_r in pure DMPC ULV is found to be very similar (14±2 μeV) [39]. At 310K, the localized translational diffusion model as described above has been used to describe the internal motion of DMPC vesicles in the presence of 0.2 mol % melittin. The variation of EISF observed at 310K can be successfully described using the Eq. (13) and (11), as shown by the solid red line in Fig. 6. The fitting parameters R_{min} and R_{max} are found to be 0.5 Å and 5.5±0.3 Å, respectively. The corresponding results for pure DMPC vesicles at 310K [39], R_{min} and R_{max} are found to be 0.1 and 5.2±0.3 Å, respectively. The unrealistically small value of R_{min} should be taken with reservation; it is merely indicative of a

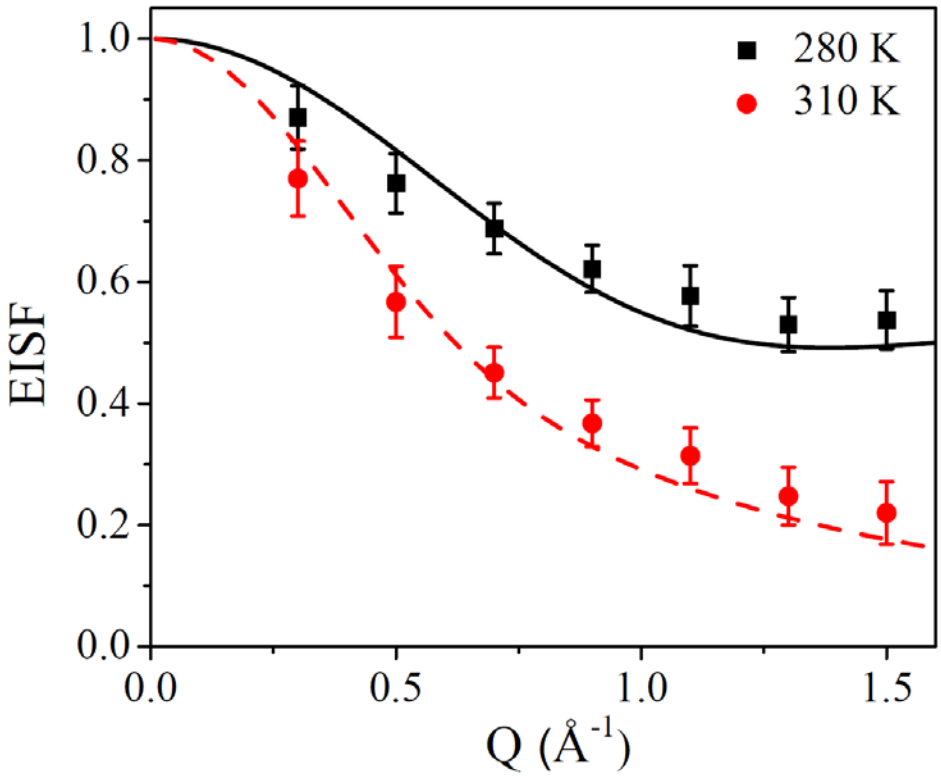

Fig. 6 Variation of EISF for DMPC ULV in the presence of 0.2 mol% melittin with Q in the solid gel (280 K) and fluid (310 K) phase. The solid and dashed lines represent the calculated EISF for uniaxial rotational and localized translational models (as discussed in the text) respectively.

negligible movement of the hydrogen atoms in the first carbon position held by the head-group. Although there is no analytical expression for the HWHM of the quasielastic part for the present model, one can calculate it numerically for given values of R_{min}, R_{max}, D_{min} and D_{max} using Eqs. (10) to (12). Assuming the present model, $D_{\min}$ and D_{max} are obtained by the least squares fitting of the data at 310 K. The values of R_{min} and R_{max} as obtained from the EISF Q-dependence (Fig. 6), kept fixed in the fitting procedure. The red solid line in Fig. 7 represents the fit as obtained from the above description, and D_{min} and D_{max} are found to be 2×10^{-7} cm^2/s and $72\pm6\times10^{-7}$ cm^2/s respectively. The obtained D_{min} and D_{max} are found to be very similar to the observed values for $D_{\min}$ (0.3×10^{-7} cm^2/s) and $D_{\max}$ ($79\pm7\times10^{-7}$ cm^2/s) for DMPC vesicles in the absence of any additive [39]. These results indicate that addition of melittin to DMPC vesicles that are in the fluid phase does not have a significant effect on the fast internal motion of lipid molecules. In

summary, the same model with slightly changed parameters is able to describe the internal motion of neat DMPC as well as DMPC/melittin. This is true for both cases below and above the phase transition temperature of the neat DMPC system. This observation suggests that the nature of the internal motion of DMPC vesicles is unaffected by the addition of melittin.

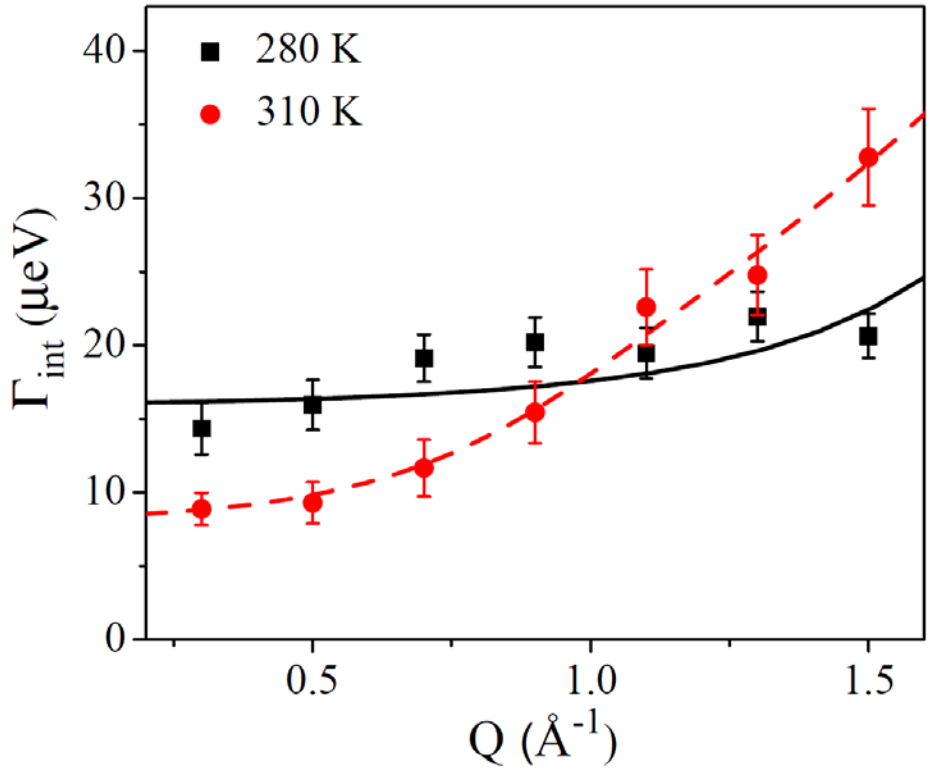

Fig. 7 Variation with *Q* of the HWHM of the Lorentzian corresponding to the internal motion, Γ_{int}, for DMPC ULV in the presence of 0.2 mol % melittin for both solid gel (280K) and fluid (310K) phases. The solid and dashed lines are the fits according to uniaxial rotational and the localized translational models, respectively.

Vesicles with Cholesterol:

The elastic intensity scans measured for DMPC ULV with 20 mol % cholesterol in the presence and absence of 0.2 mol % melittin are shown in Fig. 8a. A temperature region near the main phase transition of lipids, i.e., 296 K, is zoomed in and shown in the inset of the figure. It is evident that inclusion of 0.2 mol % melittin in the bilayer which already has been supplemented by cholesterol does not affect much the variation of elastic scan intensity with temperature.

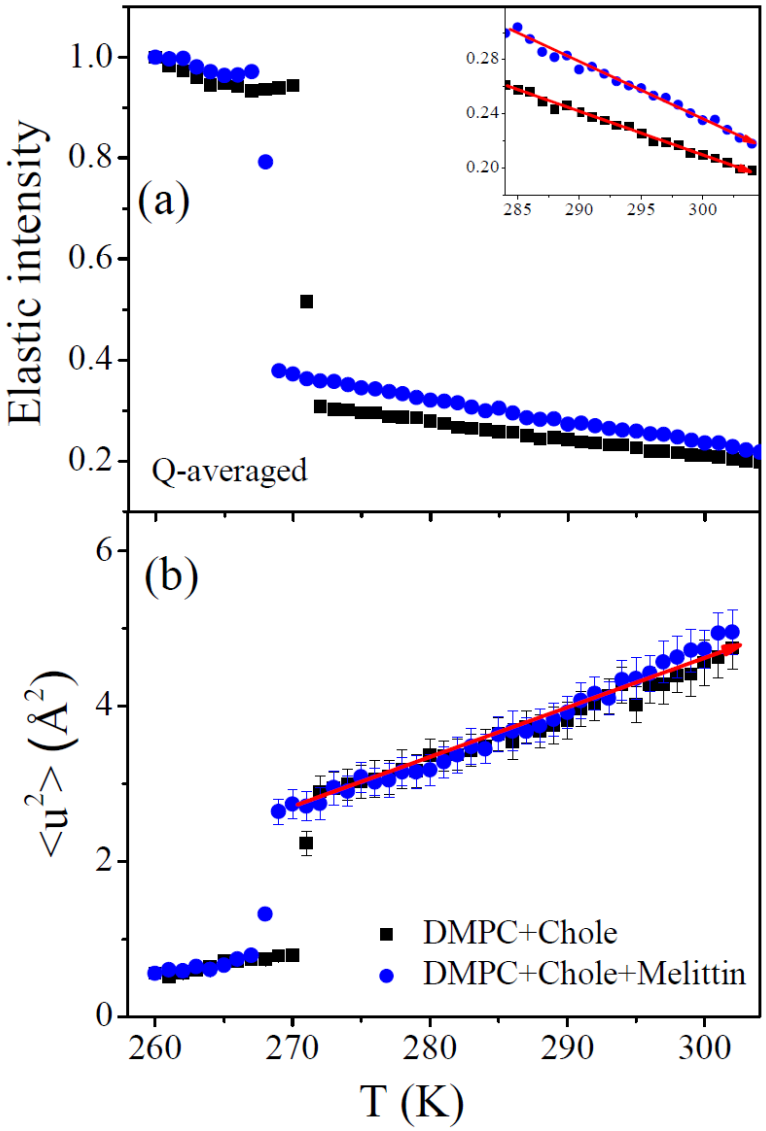

Fig. 8 Variation of (a) *Q*-averaged elastic intensity and (b) average mean square displacement $\langle u^2 \rangle$ with temperature for 74 mM DMPC ULV supplemented with 20 mol % cholesterol in the absence and presence of 0.2 mol% melittin. A region around the temperature ~296 K for *Q*-averaged elastic intensity is magnified and shown in the inset. It is evident that inclusion of 0.2 mol % melittin does not affect much the variation of elastic intensity and $\langle u^2 \rangle$, except for the transition temperature of the water buffer, which is shifted toward lower temperature. Solid red and magenta lines are drawn as guides to the eye.

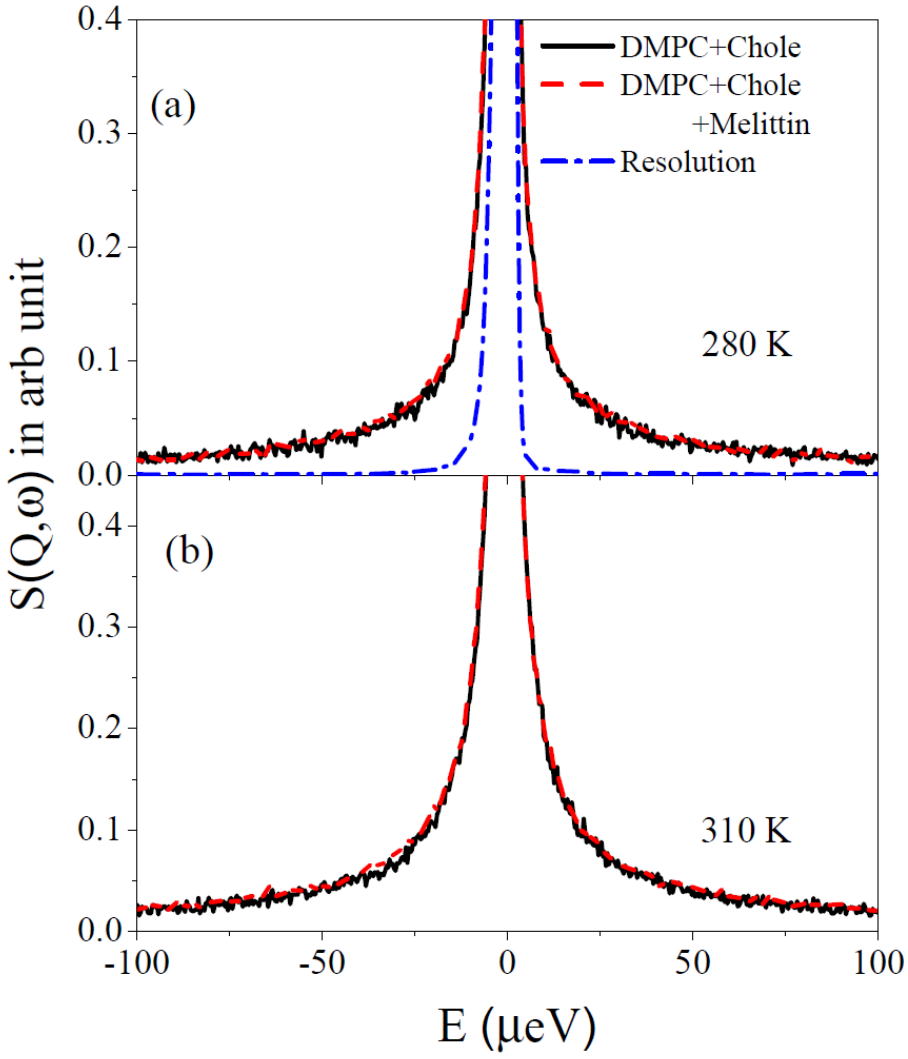

Fig. 9 Typical observed QENS spectra for 74 mM DMPC ULV containing cholesterol in the presence and absence of 0.2 mol % melittin at Q=0.9 Å^{-1} at (a) 280 K and (b) 310 K. The instrument resolution is shown by the dash-dotted line in upper panel. The contribution of the solvent (D_2O) has been subtracted using Eq. (1) and the resultant spectra are normalized to the peak amplitudes.

Moreover, no sudden drop in the elastic intensity is observed even in the case of DMPC vesicles supplemented with cholesterol only. This observation is consistent with earlier DSC measurements that indicated that addition of cholesterol causes reduction in the enthalpy corresponding to the main phase transition, and the transition becomes broader [57]. Average mean-squared displacements, $\langle u^2 \rangle$, have been extracted from the elastic

scans as described above and are shown in Fig 8b. It is also clear from Fig. 8b that addition of melittin does not have much effect on the MSD of bilayers which are already supplemented with cholesterol. These observations are in a marked contrast with the measurements with pure, cholesterol-free bilayer, where inclusion of melittin is found to affect dynamics significantly. These results suggest that presence of cholesterol in the bilayer hampers the action of melittin on the vesicles.

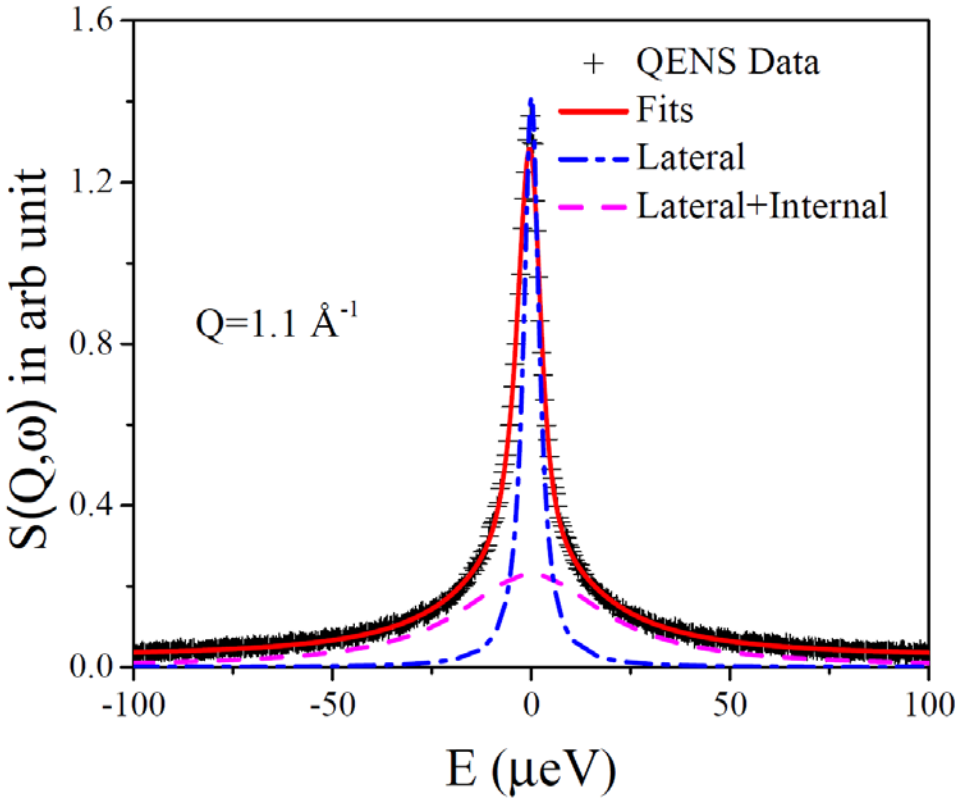

Fig. 10 Typical fitted $S_{vesicles}(Q, \omega)$ for 74 mM DMPC vesicles containing 20 mol % cholesterol with 0.2 mol % melittin at 310 K assuming model scattering function given by Eq. (5). The contribution from the solvent (D_2O) has been subtracted using Eq. (1).

QENS experiments have been carried on DMPC vesicles with 20 mol% cholesterol in the presence and absence of 0.2 mol % melittin at 280 and 310 K. The typical observed spectra are shown in Fig. 9 at a representative Q=0.9 Å^{-1}. It is evident that at both temperatures, the effect of inclusion of melittin on the DMPC bilayer which is already supplemented by cholesterol is almost negligible. These observations are consistent with the elastic scan measurements, but

provide a sharp contrast with the results obtained for pure bilayer, where melittin acts as a plasticizer at 280K and a stiffening agent at 310K. Eq. (5) can be used to separate the lateral and internal motions in the observed spectra. It is found that spectra for DMPC vesicles supplemented with cholesterol in the absence and presence of melittin can be described well by Eq. (5), and a typical fit of spectra for membranes with cholesterol and melittin is shown in Fig. 10.

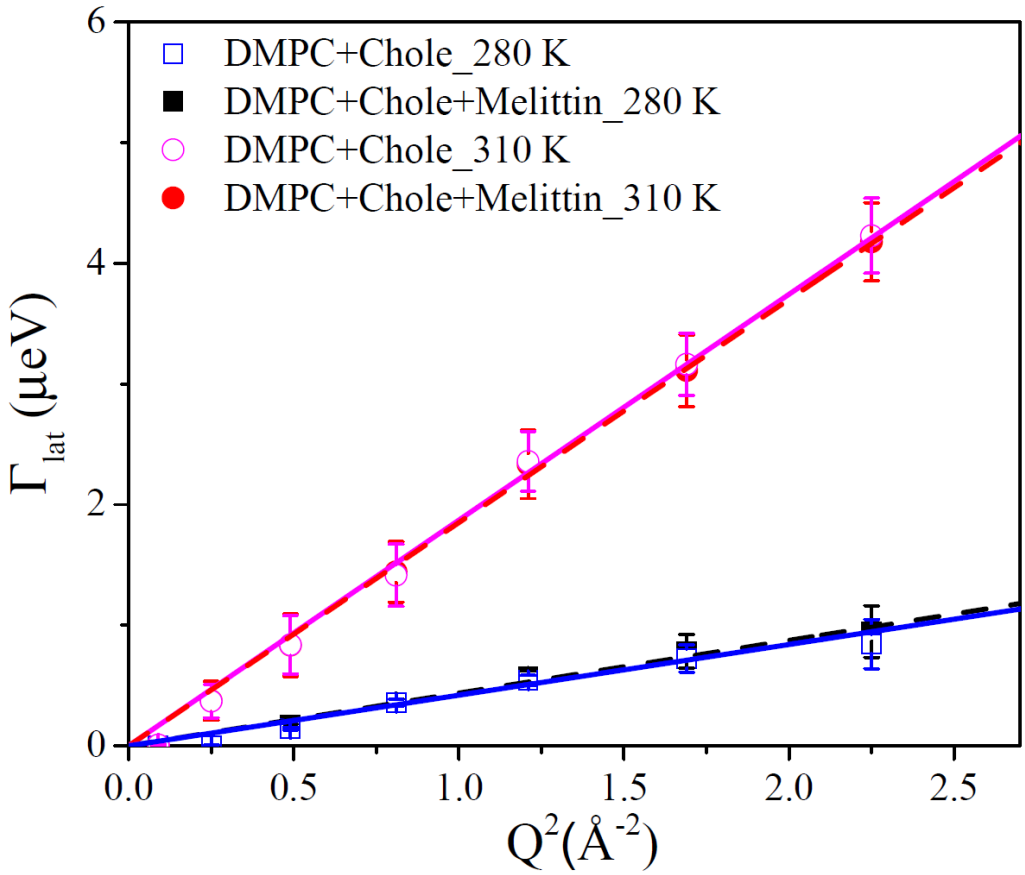

Fig. 11 Variation with Q^2 of the HWHMs corresponding to the lateral motion, $\Gamma_{lat,}$ for DMPC ULV supplemented with cholesterol in the presence and absence of 0.2 mol% melittin. The solid lines are the fits with Fick's law of diffusion.

The variation of HWHM of the first Lorentzian corresponding to the lateral motion with Q^2 is shown in Fig. 11 for DMPC with cholesterol in the presence and absence of melittin at both 280 and 310 K. It is evident that inclusion of 0.2 mol % melittin does not affect the lateral motion of lipid in the membrane which is already supplemented with cholesterol. It is found that

Fick's law can describe the variation of HWHM for both systems at both temperatures. The lateral diffusion coefficient for the membrane with cholesterol is found to be $(0.7\pm 0.1)\times10^{-7}$ cm^2/s and $(2.8\pm 0.1)\times10^{-7}$ cm^2/s at 280 and 310 K, respectively. With inclusion of melittin, D_{lat} does not change, yielding the same values of $(0.7\pm 0.1)\times10^{-7}$ cm^2/s and $(2.8\pm 0.1)\times10^{-7}$ cm^2/s at 280 and 310 K respectively. A comparison of the lateral diffusion coefficient obtained for DMPC in ULV in the absence and presence of melittin and cholesterol is given in Table 2. It is interesting to compare the lateral diffusion coefficient of DMPC in the bilayer supplemented with cholesterol vis-a-vis pure vesicles. It is evident that addition of cholesterol restricts the lateral motion of the lipid molecules, especially in the fluid phase. This could be understood since cholesterol is known to induce tight packing of lipid molecules, which may cause hindrance in the lateral motion.

Table 2 Comparison of lateral Diffusion coefficients (D_{lat}) of DMPC molecules in vesicles in absence and presence of melittin and cholesterol at 280 and 310 K.

Samples	**Lateral diffusion coefficient D_{lat} ($\times10^{-7}$ cm^2/s)**	
	280 K	**310 K**
74 mM DMPC [39]	0.7±0.1	7.7±0.3
74 mM DMPC+0.2 mol % melittin	1.1±0.1	2.4±0.1
74 mM DMPC+20 mol % cholesterol	0.7±0.1	2.8±0.1
74 mM DMPC+20 mol % cholesterol+ 0.2 mol % melittin	0.7±0.1	2.8±0.1

The presence of cholesterol in the phosphocholine reduces the binding affinity of melittin to the bilayer [58,59]. However, the fraction of membrane-bound melittin also depends on the molar ratio of lipid to peptide [58]. It has been shown [58] that for phosphocholine vesicles, binding of melittin reaches saturation at a lipid/peptide ratio of 50. However, in the presence of cholesterol (40 mol %), the fraction of bound melittin reaches saturation at higher lipid/peptide ratio (~200). In the present case, we have used lipid/peptide ratio of 500 (0.2 mol %), and therefore expect the fraction of bound melittin to be saturated in both types of vesicles (with and without 20 mol % cholesterol). It has been shown that addition of cholesterol makes the membrane more rigid [40-42], which can be quantitatively expressed as the increase in the elastic modulus or the bilayer

deformation energy of the membrane [40, 41]. Therefore, in the presence of cholesterol it becomes more difficult for melittin to penetrate inside the bilayer. This hypothesis is supported by rece

nt measurements [58] in which the depth of penetration of melittin in a bilayer was observed using a parallax method. It has been shown that melittin is localized at a relatively shallow depth in a membrane that contains cholesterol. Our CD spectra also show less alpha-helical conformation of melittin in the case of vesicles with cholesterol compared to cholesterol-free vesicles. This indicates that, in the presence of cholesterol, the folding of melittin, which is dependent on its interaction with the membrane, is inhibited. These results are consistent with the recent piezoelectric sensor and atomic force microscopy (AFM) study [59], which indicates that the presence of cholesterol in a PC membrane reduces insertion affinity constants for melittin. These observations are also supported by our elastic intensity temperature scan data, particularly in the region near the freezing point of the water buffer, which shows that in the presence of cholesterol inclusion of melittin in ULV shifts the freezing temperature of water toward the lower temperature. The likely explanation of this shift can be based on the fact that, in the case of membrane loaded with cholesterol, melittin is pushed away from the bilayer and thus interacts with the solvent. On the other hand, in the case of cholesterol-free vesicles, the inclusion of melittin does not affect the freezing temperature of the water buffer. This is because in the absence of cholesterol melittin is not expelled into the solvent, but instead is largely inserted in the bilayer.

For cholesterol-supplemented vesicles, the EISF and HWHM parameters describing the internal motion of DMPC are found to be similar in the absence and presence of melittin, indicating that internal motions are not affected by inclusion of melittin. This is the very same result as obtained for pure DMPC vesicles that the internal motion of lipid is not affected by inclusion of melittin.

Our observation suggests that interaction of melittin with a DMPC bilayer can be modulated by the physical state of the bilayer and by varying the composition of the bilayer. By addition of cholesterol, one can inhibit the disruption action of melittin on the bilayer. Our results support the notion that the rigidity of the membrane strongly influences the melittin-membrane interaction, which is in agreement with previous results [60,61].

CONCLUSION

We have performed a quasielastic neutron scattering study that allowed us to investigate various components of phospholipid motion in DMPC-based ULV through the detailed analysis of the dependence of the scattering signal on the momentum transfer, *Q*. The main goal of the study was to elucidate the effect on the phospholipid dynamics of an important antimicrobial peptide, melittin, either as a standalone additive, or in conjunction with another important cell membrane component, cholesterol, which was supplemented the membrane prior to the melittin introduction.

The present study demonstrates a profound link between the nano-scale structure and the microscopic dynamics of phospholipids in membranes. Melittin exerts great influence on the phospholipid dynamics in the cholesterol-free membrane (particularly, the lateral motions of phospholipid as a whole), acting as a plasticizer in the solid gel phase and a stiffener in the fluid phase. Cholesterol, on the other hand, acts as a stiffener only at 310 K, when pure DMPC vesicles are in the fluid phase. Remarkably, adding melittin to the cholesterol-loaded membrane does not affect the dynamics of the latter, in a marked contrast with adding melittin to the cholesterol-free membrane. At the same time, the internal, localized phospholipid dynamics, described as uniaxial rotation in the gel phase and confined diffusion in the fluid phase, are remarkably insensitive to additives. The morphological membrane changes on the nano-scale, such as formation of transmembrane pore or disruption the membrane structure, must be directly responsible for the plasticizing influence that melittin exerts on the microscopic lipid dynamics in the gel phase. However, in the fluid phase the interaction of melittin with head groups of lipid membrane is mainly responsible for the stiffening effect. On the other hand, preloaded cholesterol precludes embedding of melittin deep into the membrane, as manifested by the unchanged dynamics of the latter after addition of melittin.

Another important conclusion of the present study is that, in the multi-component systems, with more than one additive, the preferential interaction with the lipids of one additive (in this case, cholesterol), may preclude the incorporation into the membrane, and, thus, any influence on the membrane dynamics, of another additive (in this case, melittin). While studies of the effects of additives, one at a time, may be the only practical way to bypass the complexity of the real biological systems to obtain tractable results, in the complex environments of actual

cell membranes the cumulative effect of multiple additives may be quite different from the mere sum of the effects by various additives.

ACKNOWLEDGEMENTS

Research conducted at ORNL's Spallation Neutron Source, was sponsored by the Scientific User Facilities Division, Office of Basic Energy Sciences, US Department of Energy. H.O'N acknowledges support of the Center for Structural Molecular Biology funded by the Office of Biological and Environmental Research (ERKP291).

REFERENCES

1. V. Teixeira, M. J. Feio and M. Bastos, Role of lipids in the interaction of antimicrobial peptides with membranes. *Prog. Lipid Res.*, 2012, **51**, 149-177.
2. K. A. Brogden, Antimicrobial peptides: pore formers or metabolic inhibitors in bacteria? *Nat Rev Microbiol.,* 2005, **3**, 238-50.
3. M. Zasloff, Antimicrobial peptides of multicellular organisms, *Nature*, 2002, **415**, 389–95.
4. D. M. Engelman, Membranes are more mosaic than fluid, *Nature*, 2005, 438, 578–580.
5. H. Raghuraman, A. Chattopadhyay, Melittin: a membrane-active peptide with diverse functions, *Biosci Rep*., 2007, **27**, 189–223.
6. C. E. Dempsey, The actions of melittin on membranes, *Biochim. Biophys. Acta*., 1990, **1031**, 143–161.
7. Y. Shai, Molecular recognition between membrane-spanning polypeptides, *Trends Biochem. Sci.*, 1995, **20**, 460–464.
8. K. J. Barnham, S.A. Monks, M.G. Hinds, A.A. Azad, R.S. Norton, Solution structure of a polypeptide from the N terminus of the HIV protein Nef, *Biochemistry*, 1997, **36**, 5970–5980.
9. C. Golding, P. O'Shea, The interactions of signal sequences in membranes, *Biochem. Soc. Trans.*, 1995, **23,** 971–976.
10. J. F. Marcos, R. N. Beachy, R. A. Houghten, S. E. Blondelle, E. Pe´rez-Paya´, Inhibition of a plant virus infection by analogs of melittin, *Proc. Nat. Acad. Sci. USA*, 1995, **92**, 12466–12469.
11. J. Bello, H. R. Bello, E. Granados, Conformation and aggregation of melittin: dependence of pH and concentration, *Biochemistry*, 1982, **21**, 461–465.
12. J. Dufourcq, J-F Faucon, G. Fourche, J-L Dasseux, M. L. Maire and T. Guhc-Krzywlclo, Morphological changes of phosphatidylcholine bilayers induced by melittin: vesicularization, fusion, discoidal particles, *Biochim Biophys Acta*, 1986, **859,** 33-48.
13. M. Monette, M. R. van Calsteren, M. Lafleur, Effect of cholesterol on the polymorphism of dipalmitoylphosphatidylcholine/melittin complexes: an NMR study *Biochim Biophys Acta*, 1993, **1149,** 319–328.

14. S. Toraya, T. Nagao, K. Norisada, S. Tuzi, H. Saito, S. Izumi and A. Naito, Morphological behavior of lipid bilayers induced by melittin near the phase transition temperature, *Biophysical Journal*, 2005, **89,** 3214–3222.
15. S. Qian and W. T. Heller, Peptide induced asymmetric distribution of charged lipids in a vesicle bilayer revealed by small-angle neutron scattering, *J. Phys. Chem. B*, 2011, **115,** 9831–9837.
16. M. T. Lee, F. Y. Chen and H. W. Huang, Energetics of pore formation induced by membrane active peptides, *Biochemistry*, 2004, **43**, 3590–3599.
17. A. Colotto, K. Lohner and P. Laggner, Small-angle X-ray diffraction studies on the effects of melittin on lipid bilayer assemblies. *J. Appl. Cryst.*, 1991, **24**, 847-851.
18. M. T. Lee, T. L. Sun, W. C. Hung, and H. W. Huang, Process of inducing pores in membranes by melittin, *Proc. Nat. Acad. Sci. USA*, 2013, **110**, 14243-14248.
19. J. Su, S. S. Wu, U. J. M. T. Lee, A. C. Su, K.F. Liao, W. U. Lin, Y.S. Huang, C. Y. Chen, Peptide-induced bilayer thinning structure of unilamellar vesicles and the related binding behavior as revealed by X-ray scattering, *Biochimica et Biophysica Acta*, 2013, **1828**, 528–534.
20. J. Perlo, C. J. Meledandri, E. Anoardo, and D. F. Brougham, Temperature and size-dependence of molecular dynamics in unilamellar vesicles by fast-field cycling NMR relaxometry, *J. Phys. Chem. B*, 2011, **115,** 3444-3451.
21. M. F. Roberts, A. G. Redfield, and U. Mohanty, Phospholipid reorientation at the lipid/water interface measured by high resolution 31P field cycling NMR spectroscopy, *Biophys. J.*, 2009, **97**, 132-141.
22. F. Picard, M. J. Paquet, E. J. Dufourc and M. Auger, Measurement of the lateral diffusion of dipalmitoylphosphatidylcholine adsorbed on silica beads in the absence and presence of melittin: a 31P two-dimensional exchange solid-state NMR study, *Biophysical Journal*, 1998, 74, 857–868.
23. R. Macháň and M. Hof, Lipid diffusion in planar membranes investigated by fluorescence correlation spectroscopy, *Biochimica et Biophysica Acta*, 2010, **1798**, 1377-1391.

24. S. Busch, C. Smuda, L. Pardo and T. Unruh, Molecular mechanism of long-range diffusion in phospholipid membranes studied by quasielastic neutron scattering, *J. Am. Chem. Soc.*, 2010, **132**, 3232-3233.
25. S. Busch, L. C. Pardo, C. Smuda and T. Unruh, Polyaspartamide vesicle induced by metallic nanoparticles, *Soft Matter*, 2012, **8**, 3576-3585.
26. C. L. Armstrong, M. D. Kaye, M. Zamponi, E. Mamontov, M. Tyagi, T. Jenkins, and M. C. Rheinstädter, Diffusion in single supported lipid bilayers studied by quasielastic neutron scattering, *Soft Matter*, 2010, **6**, 5864-5867.
27. C. L. Armstrong, M. Trapp, J. Peters, T. Seydel, and M. C. Rheinstädter, Short-range ballistic motion in fluid lipid bilayers studied by quasi-elastic neutron scattering, *Soft Matter*, 2011, **7**, 8358-8362.
28. Y. Gerelli, V. Garcia Sakai, J. Ollivier and A. Deriu, Conformational and segmental dynamics in lipid-based vesicles, *Soft Matter*, 2011, **7**, 3929-3935.
29. M. Doxastakis, V. Garcia Sakai, S. Ohtake, J. K. Maranas and J. J. de Pablo, A molecular view of melting in anhydrous phospholipidic membranes, *Biophysical J.*, 2007, **92**, 147-161.
30. U. Wanderlingh, G. D'Angelo, C. Branca, V. Conti Nibali, A. Trimarchi, S. Rifici, D. Finocchiaro, C. Crupi, J. Ollivier, and H. D. Middendorf, Multi-component modelling of quasielastic neutron scattering from phospholipid membranes, *J. Chem. Phys.*, 2014, **140** 174901-10.
31. M. Bée, *Quasielastic Neutron Scattering*, Adam Hilger, Bristol, 1988.
32. J. H. Lee, S. M. Choi, C. Doe, A. Faraone, P. A. Pincus and S. R. Kline, Thermal fluctuation and elasticity of lipid vesicles interacting with pore-forming peptides, *Phys. Rev. Lett.* 2010, **105**, 038101.
33. J. F. Tocanne, L. Dupou- Ciézanne and A. Lopez, Lateral diffusion of lipids in model and natural membranes, *Prog. Lipid Res.*, 1994, **33**, 203-237.
34. V. K. Sharma, S. Mitra, M. Johnson and R. Mukhopadhyay, Dynamics in anionic micelles: effect of phenyl ring, *J. Phys. Chem. B*, 2013, **117** 6250-6255.
35. V. K. Sharma, S. Mitra, V. Garcia Sakai, P. A. Hassan, J. Peter Embs and R. Mukhopadhyay, The dynamical landscape in CTAB micelles, *Soft matter*, 2012, **8**, 7151-7160.

36. V. K. Sharma, S. Mitra, V. Garcia Sakai and R. Mukhopadhyay, Dynamical features in cationic micelles of varied chain length, *J. Phys. Chem. B*, 2012, **116**, 9007-9015.
37. V. K. Sharma, S. Mitra, G. Verma, P. A. Hassan, V. Garcia Sakai, R. Mukhopadhyay, Internal dynamics in SDS micelles: neutron scattering study, *J. Phys. Chem. B*, 2010, **114**, 17049-56.
38. B. Aoun, V. K. Sharma, E Pellegrini, S. Mitra, M. Johnson, R. Mukhopadhyay, Structure and dynamics of ionic micelles: MD simulation and neutron scattering study, *J. Phys. Chem. B*, 2015, **119**, 5079-5086.
39. V. K. Sharma, E. Mamontov, D. B. Anunciado, H. O'Neill and V. Urban, Nanoscopic dynamics of phospholipid in unilamellar vesicles: effect of gel to fluid phase transition, *J. Phys. Chem B*, 2015, **119**, 4460-4470.
40. P. L. Yeagle, Cholesterol and the cell membrane, Cholesterol and the cell membrane, *Biochim Biophys Acta*, 1985, **822**, 267–287.
41. C. L. Armstrong, W. Häußler, T. Seydel, J. Katsaras and M. C. Rheinstädter, Nanosecond lipid dynamics in membranes containing cholesterol, *Soft Matter*, 2014, **10**, 2600-2611.
42. D. Needham, *Permeability and stability of bilayers*, CRC Press, Boca Raton, Florida, 1995.
43. B. de Kruijff, Cholesterol as a target for toxins, *Biosci. Rep.*, 1990, **10**, 127–130.
44. A. K. Ghosh, R. Rukmini, and A. Chattopadhyay, Modulation of tryptophan environment in membrane-bound melittin by negatively-charged phospholipids: implications in membrane organization and function, *Biochemistry*, 1997, **36**, 14291–14305.
45. N. Sreerama and R. W. Woody, Estimation of protein secondary structure from circular dichroism spectra: comparison of CONTIN, SELCON, and CDSSTR methods with an expanded reference set, *Analytical Biochemistry*, 2000, **287**, 252–260.
46. Z. Yi, Y. Miao, J. Baudry, N. Jain, and J. C. Smith, Derivation of mean square displacements for protein dynamics from elastic incoherent neutron scattering, *J. Phys. Chem. B*, 2012, **116** 5028-5036.
47. L. Toppozini, C. L. Armstrong, M. A. Barrett, S. Zheng, L. Luo, H. Nanda, V. G. Sakai and M. C. Rheinstädter, Partitioning ethanol into lipid membranes and its effect on fluidity and permeability as seen by X-ray and neutron scattering, *Soft Matter*, 2012, **8**, 11839-11849.

48. E. Mamontov, K.W. Herwig, A time-of-flight backscattering spectrometer at the Spallation Neutron Source, BASIS, *Rev. Sci. Inst*., 2011, **82**, 085109.
49. J. Taylor, O. Arnold, J. Bilheaux, A. Buts, S. Campbell, M. Doucet, N. Draper et al., *Bulletin of the American Physical Society*, 2012, **57**, W26.10.
50. R. T. Azuah, L. R. Kneller, Y. Qiu, P. L. W. Tregenna-Piggott, C. M. Brown, J. R. D. Copley, and R. M. Dimeo, DAVE: A Comprehensive Software Suite for the Reduction, Visualization, and Analysis of Low Energy Neutron Spectroscopic Data, *J. Res. Natl. Inst. Stan. Technol.,* 2009, **114**, 341.
51. A. J. Dianoux, F. Volino, H. Hervet, Incoherent Scattering Law for Neutron Quasi-Elastic Scattering in Liquid Crystals. *Mol. Phys*., 1975, **30**, 1181-1194.
52. F. Volino, A. J. Dianoux, Neutron Incoherent Scattering Law for Diffusion in a Potential of Spherical Symmetry: General Formalism and Application to Diffusion Inside a Sphere. *Mol. Phys.*, 1980, **41**, 271-279.
53. Sharon M. Kelly, Thomas J. Jess, Nicholas C. Price, How to study proteins by circular dichroism. *Biochim. Biophys. Acta*, 2005, **1751,** 119 – 139.
54. J. L. Dasseux, J. F. Faucon, M. Lafleur, M. Pézolet, J. Dufourcq, A restatement of melittin-induced effects on the thermotropism of zwitterionic phospholipids, *Biochim. Biophys. Acta*, 1984, **775**, 37–50.
55. H. W. Huang, Molecular mechanism of antimicrobial peptides: The origin of cooperativity, *Biochim. Biophys. Acta*, 2006, **1758**, 1292.
56. D. Allende, S. A. Simon, and T. J. McIntosh, Multi-induced bilayer leakage depends on lipid material properties: evidence for toroidal pores, *Biophys. J.*, 2005, **88**, 1828–1837.
57. T. P. W. McMullen, N. A. Ruthven, H. Lewis, and R. N. McElhaney, Differential scanning calorimetric study of the effect of cholesterol on the thermotropic phase behavior of a homologous series of linear saturated phosphatidylcholines, *Biochemistry* 1993, **32**, 516-522.
58. H. Raghuraman, A. Chattopadhyay, Interaction of Interaction of melittin with membrane cholesterol: A fluorescence approach, *Biophys. J.*, 2004, **87**, 2419–2432.
59. L. Y. Chen, C. W. Cheng, J. Lin, W. Chen, Exploring the effect of cholesterol in lipid bilayer membrane on the melittin penetration mechanism, *Analytical Biochemistry*, 2007, **367**, 49–55.

60. E. J. Dufourc, E. J. Parish, S. Chitrakorn, I. C. P. Smith, Structure and dynamical details of cholesterol-lipid interaction as revealed by deuterium NMR, *Biochemistry*, 1984, **23**, 6062–6071.
61. A. Andersson, H. Biverståhl, J. Nordin, J. Danielsson, E. Lindahl, L. Mäler, The membrane-induced structure of melittin is correlated with the fluidity of the lipids, *Biochimica et Biophysica Acta*, 2007, **1768**, 115–121.